Pattern Recognition 43 (2010) 1476–1490

Contents lists available at ScienceDirect

Pattern Recognition

journal homepage: www.elsevier.com/locate/pr

3-D object segmentation using ant colonies

Piergiorgio Cerello [a,*], Sorin Christian Cheran [a], Stefano Bagnasco [a], Roberto Bellotti [b], Lourdes Bolanos [a,c], Ezio Catanzariti [d], Giorgio De Nunzio [e], Maria Evelina Fantacci [f], Elisa Fiorina [g], Gianfranco Gargano [b], Gianluca Gemme [h], Ernesto López Torres [c], Gian Luca Masala [i], Cristiana Peroni [g], Matteo Santoro [j]

[a] I.N.F.N., Sezione di Torino, V. Giuria 1, Torino, 10125 Italy
[b] Dipartimento di Fisica, Universita' di Bari and I.N.F.N., Sez. di Bari, Italy
[c] CEADEN, Habana, Cuba
[d] Dipartimento di Scienze Fisiche, Universita' di Napoli and I.N.F.N., Sez. di Napoli, Italy
[e] Dipartimento di Scienza dei Materiali, Universita' del Salento and I.N.F.N., Sez. di Lecce, Italy
[f] Dipartimento di Fisica, Universita' di Pisa and I.N.F.N., Sez. di Pisa, Italy
[g] Dipartimento di Fisica Sperimentale, Universita' di Torino and I.N.F.N., Sez. di Torino, Italy
[h] I.N.F.N.—Sez. di Genova, Italy
[i] Struttura Dipartimentale di Matematica e Fisica, Universita' di Sassari and I.N.F.N., Sez. di Cagliari, Italy
[j] Dipartimento di Informatica e Scienze Informatiche, Universita' di Genova and I.N.F.N., Sez. di Napoli, Italy

ARTICLE INFO

Article history:
Received 7 May 2008
Received in revised form
22 August 2009
Accepted 14 October 2009

Keywords:
Artificial life
Ant colony
Image processing
3-D object segmentation

ABSTRACT

3-D object segmentation is an important and challenging topic in computer vision that could be tackled with artificial life models.

A Channeler Ant Model (CAM), based on the natural ant capabilities of dealing with 3-D environments through self-organization and emergent behaviours, is proposed.

Ant colonies, defined in terms of moving, pheromone laying, reproduction, death and deviating behaviours rules, is able to segment artificially generated objects of different shape, intensity, background.

The model depends on few parameters and provides an elegant solution for the segmentation of 3-D structures in noisy environments with unknown range of image intensities: even when there is a partial overlap between the intensity and noise range, it provides a complete segmentation with negligible contamination (i.e., fraction of segmented voxels that do not belong to the object). The CAM is already in use for the automated detection of nodules in lung Computed Tomographies.

1. Introduction

Ant Colony Models are computational simulations of ant colonies that use the behaviour rules observed in nature to design cooperation/competition strategies to be put in place by virtual agents: the emergence of a global *smart* behaviour and a *purposive* self-organization can then be exploited to solve difficult problems.

Successful applications of Ant Colony Models range from optimization techniques [1,2] to swarm robotics [3]. The use of Ant-Colonies in image processing, pattern recognition and object segmentation (usually tackled with classical algorithms such as region growing, active contour and shapes models, watershed transformations, genetic algorithms, etc.) started in the nineties [4]. Many solutions for 2-D image segmentation, thresholding and processing were developed but few of them were used in a 3-D environment [5–8]. Ant Colony Models are intrinsically 3-D, since all the activities performed by an ant super-organism, like forging, larvae feeding, nest building, etc. take place in a 3-D environment [9].

The approach we propose, called *Channeler Ant Model*, is a stable and elegant solution that requires little tuning (parameter-wise), provides an excellent performance on images with different dynamic ranges and noise levels and opens a multitude of possibilities for further research. The present work was carried on within the MAGIC-5 Project [10], focused on the development of algorithms for the automated detection of anomalies in medical images. The *Channeler Ant Model* discussed here is being adopted as a tool for the analysis of lung CT scans [11–13], as a way to segment and remove the background coming from the bronchial and vascular trees in the lungs, which is the biggest source of false positive findings in the automated search for nodules.

* Corresponding author. Tel.: +390116707416; fax: +390116699579.
E-mail address: cerello@to.infn.it (P. Cerello).

0031-3203/$ - see front matter © 2009 Elsevier Ltd. All rights reserved.
doi:10.1016/j.patcog.2009.10.007

2. Methods and literature

2.1. Modelling ants

In [1] Bonabeau et al. clearly define the difference between modelling and designing a biological model, i.e., between a true understanding of the ant social behaviour and a mere implementation of some aspects of the natural systems. According to the authors, when thinking about modelling one tries to uncover and understand what happens in an ant colony and how its emergent behaviour really appears. Every aspect of the model must be supported by biological reasoning. Many aspects of the colony emerging behaviour like path optimization when forging for food [14,2], raiding patterns formation [15], labour and task division [16], cemetery organization [17], etc. can be modelled.

2.2. Ants in a 3-D environment

Social insects form a decentralized super-organism composed of many cooperative, independent, sensory-motor equipped components that are spread in the environment and respond to external stimuli based on local information that can come either from the environment itself or from other nest mates. The perception of the colony is the sum of perceptions of all its members, while the colony behaviour is the sum of all the interactions between the ants and the environment and between themselves. All the activities like forging, cemetery building, larvae feeding and brood sorting take place in the 3-D world perceived by the individuals [9].

One of the most complex tasks performed by social insects is nest building. Ants were initially thought to be anthropomorphic,[1] as if each individual had a 3-D blue print of the global structure embedded into its *memory*: based on that hypothesis, ants should be able to optimize their decisions and thus the nest complexity would be the result of the complexity of the insect behaviour. The observation of colonies showed that ants are not anthropomorphic and the amazing nest complexity is the consequence of the variety of stimuli to which the individual ants are subjected and respond. At the beginning of nest building, the behaviour and the type of response to the stimuli is very simple and unique: an ant carrying a pebble that finds a rock on its path will drop its load and start searching for similar items, so that piles grow bigger, attract more ants and the construction evolves. In a following phase, the types of stimuli diversify and so does the type of possible responses, leading to job diversification and to an increased nest complexity.

However, even though ants are not anthropomorphic, the nest blue-print does exist: not at the level of each individual but as a template found in the environment in the form of physical and chemical heterogeneity that helps organizing the building activities. The process, called stigmergy[2] and introduced by Grasse in [18], alongside self-organization helps ants deal with 3-D structures.

2.3. Ants in images

Chialvo and Millonas [4] introduced one of the simplest and most efficient models of trail forming when the ants are not moving in a closed boundary and are not suppressed by other behaviour rules. They compared the *trail leaving* technique with the cognitive map patterns from brain science, with the difference that ants leave their trails in the environment while the "mammalian cognitive maps lie inside the brain".

Based on the above paper, Ramos and Almeida [19] developed an extended model where a constant population of ants is deployed in a digital habitat (i.e., an image) that the insects perceive and in which they move: they showed that ants are able to react to different types of digital habitat, achieving in the end a global perception of the image as the sum of the local perceptions of the single colony members.

In the model evolution [20,21] a mechanism that self-regulates the population by using the concepts of ageing, death and reproduction in the ant colony is described. The work of Ramos and Almeida is at the root of the model we present in this paper.

Bocchi et al. [6] proposed an image segmentation method that makes use of an evolutionary swarm-based algorithm in which different populations of individuals compete to occupy the 2-D image to be analysed. The comparison to other techniques showed an improvement in the segmentation of noisy images. Zhuang et al. proposed in [5] a swarm intelligence technique for feature extraction in image processing, based on Dorigo's *ant colony system* [1] and the perceptual graphs [22] that represent the relationship between adjacent points in the image. The *ant colony system* is used to extract just the perceptual graph that afterwards becomes the basis for a layered model of a machine vision system used for the feature extraction. A method for hierarchical image segmentation, represented by a binary tree, is introduced in [23], while in [7] Malisia et al. used ant colony optimization for image thresholding. Another method for image segmentation using behaviour agents that breed and diffuse according to the image intensity is found in [8]. George and Wolfer [24] presented a swarm intelligence based method for the counting stacked symmetric objects in digital images.

As seen from the above papers, the literature provides many examples of ant colonies implementation in 2-D images based on different algorithms: ant colony systems, perceptual graphs and binary trees. Unfortunately none of them were scalable or could be applied in 3-D imaging with unknown image intensity range.

3. The Channeler Ant Model

The deployment of ant colonies in 3-D images could in principle be very effective whenever complex connected structures, with several ramifications of different size and intensity, must be identified and reconstructed, as long as a general model with few requirements on parameter tuning is designed and validated on images with known properties (different signal to background ratio and intensity range).

The development of the *Channeler Ant Model* (CAM) was triggered by the idea of using it for the automated search of suspect nodules in lung computed tomographies: the CT analysis makes use of the CAM to segment the bronchial and vascular tree and remove it from the CT before the search for nodular structures in the image with a dedicated filter or with the CAM itself [11,12].

In a way the CAM could be considered an extension of existing models [4,19,20], but it also introduces important new features.

Chialvo and Millonas [4] make use of the concept of *probabilistic directional bias*. The probability of a voxel to become the ants destination is increased when the ant keeps its direction and such effect is convoluted with the pheromone density in the definition of a new ant location. Moreover, the ant population is static (there is no evolution driven by birth and death of ants) and the initial positions are selected randomly. The model described in [4] was adopted as a starting point by Ramos and Almeida [19], who introduce a correlation between the quantity of pheromone

[1] Having human characteristics.

[2] Method of communication in emergent systems in which the individual parts of the system communicate with one another by modifying their local environment.

that is released and the pixel intensity, a feature that is also exploited by the CAM and allows the search for different image features depending on the choice of the pheromone release function. Ramos et al. [20] improve the model presented in [19] by adding a self-regulation mechanism to the ant population. However, the probability to produce an offspring is related to the number of neighbour ants, a feature that does not optimize the environment exploration: by definition, ants that lead the exploration do not have the highest number of neighbours. The probability of dying increases with the lifetime, but unless it does it rapidly enough it can cause an overcrowding in certain image volumes, since no pheromone saturation mechanism that forbids destinations is implemented. In the CAM, the *energy* parameter that regulates the lifetime of ants changes according to the local properties of the environment and defines a range within which ants live: above the higher threshold they reproduce, below the lower one they die. With that approach, the *forward leading ants* probability of reproducing can be high and the environment exploration is faster.

Existing models, although extendable to a 3D environment, did not provide a satisfactory set of rules for the use of ant colonies in images as complex as lung computed tomography. The *Channeler Ant Model* makes use of basic concepts introduced by other models [4,19,20] but it changes their implementation in a relevant way:

- the ants are not set at random positions but start the exploration from an anthill;
- the moving rules only depend on the pheromone content at destination, i.e., there is no *directional bias*;
- the lifetime is regulated by a double threshold in *energy* to define reproduction and death and the number of ants generated at each offspring depends on the pheromone configuration in the surroundings;
- the ant colony behaviour is related to the original image features only via its influence on the pheromone release rules;
- the exploration is guaranteed by a pheromone saturation mechanism, that also provides an intrinsic normalization. The maximum pheromone content of a *voxel* is set by a user-defined threshold and does not depend, in the well-explored volume, on the original image range of intensity. Moreover, whenever the pheromone content of a *voxel* is above threshold, it becomes a forbidden destination.

3.1. The colony members

The behaviour of ants, partially derived from [4,19], is described in terms of four modules: the *moving* rules, the *pheromone laying* rules, the *reproduction/death* rules and the description of the ant response to anomalies (*deviating behaviour*).

Ants explore (i.e., "live in") a 3-D spatial environment described in terms of the properties (position, intensity) of discretized VOlume ELements (*voxels*) and their life cycle is defined in terms of atomic time steps, during which ants move from one *voxel* to a neighbour.

So, at time t an ant k is in *voxel* v_i; after one life cycle (time $t+1$) it will move to *voxel* v_j. In a 3-D environment, a *voxel* has 26 first order neighbours according to Moore's neighbouring law [25].

Two types of individuals live in a colony: the *queen* and the *worker* ant.

The *queen* acts as an observer, performing tasks related to the colony coordination such as deciding when an ant dies or new ants are born.

The *workers* carry out the nest building (i.e., the objects segmentation): they move in the habitat and lay pheromone according to its properties and the model rules. Therefore, the following perspectives are possible:

(1) the Designer's (*Planner*)—it envisages the final purpose of the algorithm, which by means of the ant colony tries to achieve the reconstruction of 3-D objects by defining a set of rules that drive the colony evolution: it therefore plans the *bigger picture*, specifically by means of choosing the laying rule that correlates the released pheromone amounts to the intrinsic environment properties (i.e., the *voxel* intensities);
(2) the Queen's (*Observer*)—from its point of view the final purpose of the algorithm is not interesting nor foreseen; the important point is the supervision of the colony evolution. The *queen* has a global view of the entire habitat but it cannot interfere, change it in any way nor directly tell the working units what they are supposed to do, which direction to choose, *etc*. In other words, the *queen* can see the *bigger picture* but is not allowed to set specific aspects or change the colony rules. The *queen* implements the pheromone map analysis (see the following sections) and therefore makes use of the global knowledge to decide whether *voxels* are part of the segmented structure or not.
(3) the Ant's (*Executor*)—it is local, as the single *ant* only perceives the local environment properties at a given time unit and follows the behaviour rules. The *ant* has no idea of the global colony status, evolution or goal: it focuses on completing its given tasks with no regard to the emergent behaviours that might appear in the overall colony.

3.2. The ant colony rules

The behaviour of *worker* ants is defined by a set of rules that specify how they move in the environment, how much pheromone they release before moving to another location, when they reproduce or die, how they react to anomalies (e.g., when they reach the environment boundaries): the modelling of each of these rules is discussed in the following subsections.

The environment is essentially defined by the *voxel* image intensities, which can be thought of as related to the amount of available food for the colony, which should be progressively consumed when the number of visits increases. This mechanism, required to make the colony evolve and explore the environment, is implemented in a complementary way: whenever the limit to the maximum number of visits (N_V) in a *voxel* is reached, the *voxel* is no more available as a destination.

3.2.1. The moving rules

Randomness is an important factor in self-organization as it can assure a good balance between following a well established path and the probability of finding new and better paths, triggering the exploration of new regions of the environment.

Like in nature, in the CAM the random component associated to the way an ant walks is taken into account for the choice of the future destination.

However, the choice of the direction for a step must also take into account the colony global knowledge of the environment, which is provided by the amount of pheromone already released is a given position (σ_j). The pheromone laying rules are analysed in the following, but the meaning of a pheromone message is the same as in nature: a large amount of pheromone in a candidate destination must correspond to a high probability of becoming the actual destination.

Ants make one step per life cycle: therefore an ant k located in *voxel* v_i at time t must select its destination. The choice is made according to the following rules:

- only the $n=26$ first order neighbours are destination candidates;
- for each *voxel* neighbour v_j, a probability P_{ij} for it to be chosen as destination is computed;
- if an ant is detected in v_j, P_{ij} is set to zero;
- once a probability of becoming the future destination is assigned to each candidate, one of them is selected by a roulette wheel algorithm.

The probability P_{ij} that a candidate destination is chosen is defined as follows:

$$P_{ij}(v_i \to v_j) = \frac{W(\sigma_j)}{\sum_{n=1,26} W(\sigma_n)} \tag{1}$$

where $W(\sigma_j)$ depends on the amount of pheromone in *voxel* v_j and the denominator is a normalization factor.

The pheromone-related term $W(\sigma_j)$, taken from [4], depends on the *osmotro-potaxic sensitivity* β (the larger it is, the larger the influence of the pheromone trail in deciding the ant's future destination) and on the sensory capacity $1/\delta$ (if the pheromone concentration is too high, it will determine the decrease of the ant's capability of sensing it):

$$W(\sigma_j) = \left(1 + \frac{\sigma_j}{1+\delta\cdot\sigma_j}\right)^{\beta} \tag{2}$$

A random number selected in the (0,1] interval determines which *voxel* is actually selected as destination.

3.2.2. Pheromone laying rules

According to the biological laws of ant colonies, before moving to the future destination an ant k deposits in the *voxel* it is about to leave a quantity of pheromone T, defined as [19]

$$T = \eta + \Delta_{ph} \tag{3}$$

where η is a small quantity of pheromone that an ant would leave anyway and Δ_{ph}, the differential quantity of the pheromone, links the image properties to the pheromone habitat in which the ants live. Its value is a *voxel*-intensity dependent function:

$$\Delta_{ph} = \Psi(I) \tag{4}$$

The choice of the depositing rule, made at the *Planner* level, is very important as it is related to the type of segmentation the ants are going to perform. Some possible choices of Δ_{ph} for an ant that moves from *voxel* v_i to v_j with intensities $I(v_i)$ and $I(v_j)$ are shown below:

$$\Delta_{ph} = const\cdot I(v_i) \tag{RuleI}$$

$$\Delta_{ph} = const\cdot |I(v_i) - I(v_j)| \tag{RuleII}$$

$$\Delta_{ph} = const\cdot \frac{\sum_{l=1}^{n'} I(v_l)}{n'} \tag{RuleIII}$$

where n' is the total number of neighbours including the starting *voxel*: $n' = n+1 = 27$ since only first order neighbours are considered.

Rule I, in which the ant lays a quantity of pheromone directly proportional to the intensity of its starting *voxel*, is used for the segmentation of objects on a background (e.g., the case of lung computed tomographies); *Rule II*, with a pheromone release proportional to the intensity derivative, can be used for border detection (e.g., the search for the pleura in lung CTs); *Rule III* smooths the effect of the intensity fluctuations and can therefore be used for segmenting objects in a noisy environment whenever the noise fluctuates more than the signal. In the results section, only Rule I is addressed: however, it is important to remark that, just by changing the pheromone deposition rule, it is possible to enhance different image features.

After depositing the pheromone according to the implemented rule, the ant moves to the selected destination *voxel*.

3.2.3. The life cycle—reproduction and death

Ants, like all the living creatures, live for a finite amount of time. The life cycle is regulated by a parameter called energy [21], which is assigned at birth with a default value:

$$\varepsilon_0 = 1+\alpha \tag{5}$$

The energy variation for ant k must take into account the properties of the environment, which are defined by the deposited amount of pheromone Δ_{ph}^k for the current cycle and by the average amount of pheromone per step the colony has deposited since the beginning of its evolution, used as a normalization factor ($\langle \Delta_{ph} \rangle$): Fig. 1 shows that the integrated average, used for the normalization, converges to a constant factor and is far more stable than the average per cycle. Therefore, the energy variation for ant k is defined as follows:

$$\varepsilon_{t+1}^k - \varepsilon_t^k = -\alpha\cdot\left(1 - \frac{\Delta_{ph}^k}{\langle \Delta_{ph} \rangle}\right) \tag{6}$$

The energy range is defined by a lower limit, the death energy ε_D and an upper limit, the reproduction energy ε_R: an ant with energy ε_t^k will die whenever $\varepsilon_t^k < \varepsilon_D$ and give birth whenever $\varepsilon_t > \varepsilon_R$. In that case, the ant energy is reset to the default starting value ε_0. The ant life cycle duration is therefore a function of the ratio between the rate of the energy variation (α) and the amplitude of the allowed energy range ($\varepsilon_R - \varepsilon_D$), all of it modulated by the properties of the environment.

The number of ants that are generated when a reproduction takes place ($N_{offspring}$) must be related to the local properties of the environment, known through the pheromone map generated by the colony, and take into account the number of free destination *voxels* (n_f).

The local properties of the environment are evaluated by smoothing the pheromone map at $v_0 = v(x_0, y_0, z_0)$ and replacing T with T_5, the pheromone release evaluated according to the selected deposition rule when the *voxel* intensity I is replaced by I_5, defined as the average intensity in the *voxel*'s 125 second

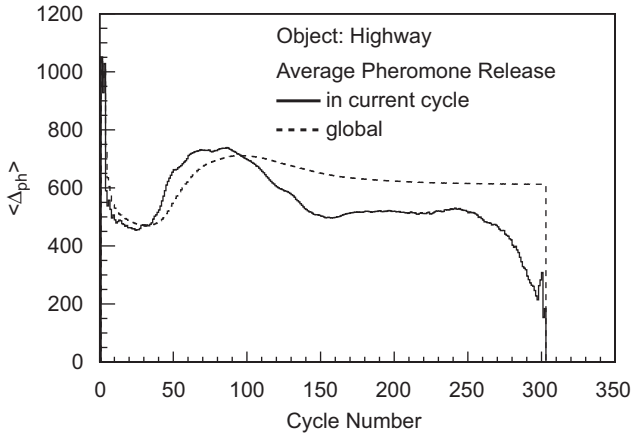

Fig. 1. The average pheromone release as a function of the cycle number: per cycle (full) and integrated (dashed). The integrated average release becomes more and more stable as the colony evolves and is therefore suitable for use as a normalization factor.

order neighbours:

$$I_5(v_0) = \frac{1}{125} \sum_{x_i,y_i,z_i=-2,2} I(x_0+x_i, y_0+y_i, z_0+z_i) \quad (7)$$

For each image, $T_{5,min}$ and $T_{5,max}$ are defined as the smallest and largest values of T_5, respectively. The number of generated ants can be an integer in the $[0,26]$ interval, since only first order neighbours are allowed as positions for the generated ants. The actual number $N_{offspring}$ is determined assuming that it linearly depends on T_5, with $N_{offspring} = 0(26)$ corresponding to the minimum ($T_{5,min}$) and maximum ($T_{5,max}$) taken by T_5, respectively:

$$N_{offspring} = 26 \cdot \frac{T_5(v_i) - T_{5,min}}{T_{5,max} - T_{5,min}} \quad (8)$$

In case $N_{offspring}$ is larger than the number of free neighbours n_f, it is set to n_f.

3.2.4. The deviating behaviours

Some conditions, not compatible with the above-described rules, require the definition of the allowed *deviating behaviours*. In particular:

- when an ant is fully surrounded by fellow mates and any possible destination *voxel* is unreachable, the ant is killed;
- when an ant reaches the border of the habitat it is killed.

3.3. Deploying the model

The Channeler Ant Model, discussed in the previous section, can be easily translated into an algorithm for 3-D image segmentation, which hereafter is referred to as the *CAM algorithm*. It is worth pointing out that the CAM algorithm output is not a segmented image but rather a pheromone map, which can be considered an effective preprocessing of the 3-D volume for the actual segmentation, which is discussed in the following and it is actually provided by the analysis of the pheromone map. The *CAM algorithm* input–output interface is the following:

Input:
(1) *InputImage* [A 3-D image, i.e., a collection of N 3-D voxels v_i]
(2) N_v [Maximum number of visits for each voxel]
(3) N_A [(Initial) number of Ants in the colony]
(4) v_{AH} [Anthill position, i.e., the voxel where the colony starts building the nest]
Output:
(1) *PheromoneMap*: a 3-D volume that stores the amount of pheromone released by the ants in each voxel v_i of the original image.

Some auxiliary data structures are to be defined in order to understand the pseudo-code, shown in Fig. 2:

Auxiliary data structures:
(1) *NumVisits*: an array that stores the number of times an ant has visited a specific voxel.
(2) *Ant*: a dynamic data structure used to conveniently manage ants births and deaths in the colony.
Each ant is described by its position $Ant(v_i)$ and energy $Energy(Ant(v_i))$.
Auxiliary functions:
(1) *EvaluateCandidateDestination* (v_i, v_j): implements Eqs. (1) and (2).
(2) *DifferentialPheromone* $(InputImage, v_i)$: implements Eq. (4) on the basis of the selected laying rule of Section 3.2.2.
(3) *SelectDestination* (P_{ij}): selects the actual destination from the probability map P_{ij}.
(4) *Move* $(Ant(v_i), v_j)$: moves the ant from voxel v_i to v_j.
(5) *UpdateEnergy* $(Ant(v_i), \Delta_{ph})$: implements Eq. (6), requiring the differential amount of pheromone deposited in the current cycle.

According to the pseudo-code (Fig. 2), the model deployment goes as follows:

- initially, at $t=0$, all the *voxels* are pheromone free: no information is available to the ants for their evolution;
- an initial ant-hill is chosen in a *voxel* that belongs to the structure to be segmented and $N_0 = 26$ ants are released in all directions (i.e., in all the anthill neighbours) with default energy;
- the ants start moving around in the environment according to the above described CAM rules and deposit pheromone;
- the selected rule for depositing pheromone is defined with the goal of segmenting high intensity regions: $\Delta_{ph} = const \cdot I(v_i)$, where $I(v_i)$ is the intensity of the *voxel* on which the ant stands;
- a cycle is finished when all the ants in the population have made one move;
- after a cycle is completed, the ants energies are updated and compared to ε_D and ε_R;

1 *The CAM Algorithm*

```
t ← 0
Colony ← {}
for all v_i ∈ InputImage do
  NumVisits(v_i) ← 0
  PheromoneMap(v_i) ← 0
end for
for all v_i ∈ Neighbours(v_AH) do
  Colony ← Colony ∪ {Ant(v_i)}
  NumVisits(v_i) ← NumVisits(v_i) + 1
end for
while (N_A > 0) do
  t ← t + 1
  for all Ant(v_i) ∈ Colony do
    for all v_j ∈ Neighbours(v_i) do
      P_ij ← EvaluateCandidateDestinations(v_i, v_j)
    end for
    Δ_ph ← DifferentialPheromone(InputImage, v_i)
    P_ij
    PheromoneMap(v_i) ← PheromoneMap(v_i) + Δ_ph(Ant(v_i))
    v_j ← SelectDestination(P_ij)
    Move(Ant(v_i), v_j)
    NumVisits(v_j) ← NumVisits(v_j) + 1
  end for
  for all Ant(v_i) ∈ Colony do
    Energy(Ant(v_i)) ← UpdateEnergy(Ant(v_i), Δ_ph)
    if Energy(Ant(v_i)) ≤ ε_D then
      Colony ← Colony/A(v_i)
      N_A ← N_A − 1
    end if
    if Energy(Ant(v_i)) ≥ ε_R then
      {v_1, ..., v_k} ← RandomSampleFrom(Neighbours(v_i)).
      Colony ← Colony ∪ {Ant(v_1), ..., Ant(v_k)}
      N_A ← N_A + k
      for all j ∈ {1, ..., k} do
        NumVisits(v_j) ← NumVisits(v_j) + 1
      end for
    end if
  end for
end while
```

Fig. 2. The Channeler Ant Model segmentation algorithm Pseudo-code.

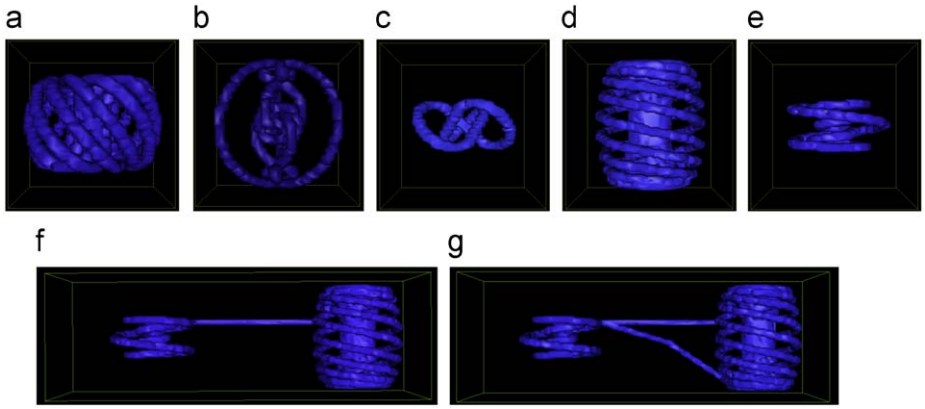

Fig. 3. The artificial objects shapes used for the model validation: (a) the toroid, (b) the knot, (c) the highway, (d) the yo-yo, (e) the scale, (f) the 1-Arm bridge, (g) the 2-Arm bridge.

- if a death is triggered then the ant is killed and the number of members in the population updated;
- if an offspring takes place, the newborn ants are placed randomly in free neighbouring *voxels* with default energy and the colony population is updated;
- the colony lives and moves until no more ants are alive or until the user-predefined number of cycles has been completed;
- once the colony evolution stops the 3-D pheromone map is stored and analysed.

4. Testing the model

4.1. The artificial images

The task of a CAM colony is to provide 3-D pheromone maps of the explored volume, to be used as a starting point for the segmentation of structures. In order to assess the model performance, it is important to study its results on a set of artificially generated 3-D objects with different shape, known properties (intensity distribution, background level), in three groups of increasing complexity:

- *Class-A set*: homogeneous intensity ($I = I_0$) objects with zero background;
- *Class-B set*: objects with heterogeneous intensity extracted from a Gaussian with μ_I average and σ_I standard deviation and zero background;
- *Class-C set*: objects with heterogeneous intensity extracted as for the *Class-B* set and a background noise extracted from a Gaussian with μ_{noise} average and σ_{noise} standard deviation.

The implemented shapes, some of them shown in Fig. 3, were selected to test the model behaviour in different conditions: the *highway* tests that ants truly channel in 3-D; the *scale*, *knot*, *toroid* and *yoyo* test the channelling through an object that constantly changes orientation; the *bridges* define the colony reaction to thin multi-branch structures. Moreover, an example of a 2-D object (the *snake*, shown in Fig. 4) was also selected to demonstrate that the model performance in 2-D and 3-D is comparable, as it is expected according to the model design.

Each object was simulated in three versions, according to the specifications of classes A, B and C. Table 1 summarizes the size and the total number of *voxels* of the different generated 3-D (2-D) images as well as the number of *voxels* that are actually part of the artificial object.

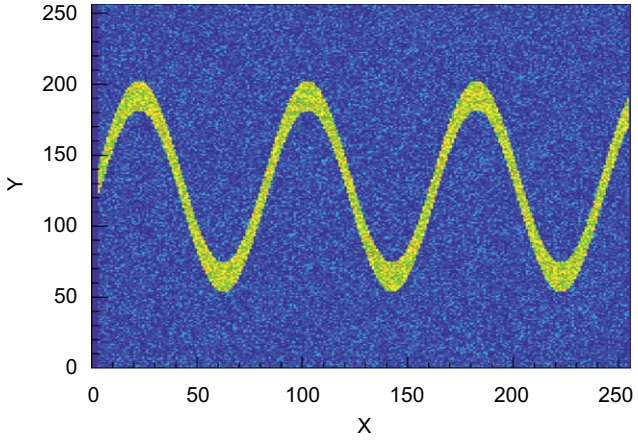

Fig. 4. The 2-D artificial snake used for the model validation.

Table 1
Artificial objects properties: the 3-D (2-D) image size in the X, Y, Z directions (N_X, N_Y, N_Z), the number of *voxels* in the image (N_{Tot}) and the number of *voxels* belonging to the generated objects (N_{Object}).

Object	N_X	N_Y	N_Z	N_{Tot}	N_{Object}
Highway	80	80	80	512000	6800
Scale	80	80	80	512000	10824
Knot	80	80	80	512000	16659
Toroid	80	80	80	512000	30332
Yoyo	80	80	80	512000	45116
1-Arm-Bridge	240	80	80	1536000	56677
2-Arm-Bridge	240	80	80	1536000	57522
Snake (2-D)	256	256	1	65536	5292

4.2. The lung CT images

As quickly addressed in the Introduction, the model was developed having in mind its use as a module of a lung Computer Assisted Detection tool, aiming at the identification of nodules in lung computed tomographies. In particular, the CAM is responsible of the segmentation of the bronchial and vascular trees in the lung, so as to be able to remove them from the original images and search for nodules in conditions that reduce the number of false positive candidates.

Although it is beyond the goal of this paper to discuss in detail the performance on real lung CTs, which requires a careful definition of the radiological *truth* according to medical protocols,

an example of pheromone map obtained on a real lung CT will be shown in the following. However, the definition of a metric to quantify the CAM performance in lung CTs is not addressed in this paper, as it is strongly related to the radiologists' diagnosis and the far from obvious definition of a *gold standard*. A discussion of the problem, as well as a very detailed discussion of the CAM (and other algorithms) results on lung CTs as a function of the different types of nodules, is found in [11,12].

4.3. Parameters optimization

The colony evolution is a function of several parameters that describe:

- the way an ant computes the perceived pheromone quantity from a *voxel*, based on Eq. (2) that contains two parameters: β and δ. In [19] the authors discovered the emergence of well defined networks of trails with $\beta = 3.5$, $\delta = 0.2$, the values we decided to adopt.
- the way an ant deposits pheromone in the *voxel* it is about to leave, set according to Eq. (3). The default quantity of pheromone that an ant leaves behind (η), which only certifies a *voxel* was visited, must be small; it is defined in such a way that it is always negligible if compared to pheromone releases relevant for the definition of a *voxel* as *segmented*:

$$\eta = 0.01 \tag{9}$$

- the way the ant energy is updated, according to Eqs. (5) and (6): α is a constant that ensures that each ant makes at least a few moves before dying, while the scale factor that determines how quickly the energy of an ant will increase or decrease, thus deciding how fastly the reproduction and death take place, is defined in terms of the local habitat properties.
  The critical issue is related to the necessity to find a satisfactory equilibrium between two different effects: the capability to explore new, pheromone free volumes and the minimization of the so-called *tunnelling*, which causes ants reach unconnected structures. For example, in the case of the *Toroid-B*, the coils of the object are so close to one another that, unless the model parameters are properly tuned, they can be reached by ants that tunnel from a neighbouring coil through an empty (i.e., low intensity) volume.
  The maximum number of steps travelled by an ant in a pheromone free region is given by

$$N_{steps} = (\varepsilon_R - \varepsilon_D)/\alpha \tag{10}$$

  In order to minimize *tunnelling*, N_{steps} must be small. In the present work, the ε_D, ε_R and α parameters were set to 1.0, 1.3, 0.2, respectively: therefore, in pheromone free areas, no more than two steps can be travelled.

The limitation to the number of visits a *voxel* can receive (N_V), introduced in order to make the colony evolve in time along the structures to be segmented, is not to be considered a model parameter. Its upper limit defines the speed with which structures are segmented, not the capability of ants to segment them.

The lower limit must take into account that the number of visits a *voxel* receives is also related to the exploration of its surroundings: since the definition of the ants future destination is probability-based, N_V must be large enough to allow a statistically significant number of moves to all the neighbours of any visited location.

In other words, N_V should be *voxel*-dependent and its value must be inversely related to the pheromone release in that *voxel*, which in turn depends on the selected laying rule, so that in areas with small depositions a larger number of visits is allowed, increasing the statistical significance of the results. With N_V ranging in the 40–120 interval, a generic v_i to v_j step takes place about 1.5 (4.5) times in high (low) deposition regions, which proves to be enough for a satisfactory segmentation. For any given image, the pheromone deposition in each *voxel* can be easily determined: assuming it ranges in the whole image from T_{min} to T_{max}, the maximum number of visits for a *voxel* is *normalized* as follows:

$$N_V = 40 + 80\frac{T - T_{max}}{T_{min} - T_{max}} \tag{11}$$

In case the pheromone laying rule also depends on the ant destination, T is meant to be the release averaged over all the possible destinations.

5. Results

Once the model parameters were optimized, the CAM was deployed on 3-D artificial objects belonging to classes A, B, C.

The choice of the simulated object properties (intensity and background) was driven by the goal of testing the CAM performance as a function of the object intensity (average and standard deviation) and background dispersion (i.e., noise). Therefore, different object sets were generated, as summarized in Table 2.

Each time an ant colony life cycle is completed, a pheromone map of the original image is available for the analysis, as well as a map of the number of visits each *voxel* received: Fig. 5 shows some samples of 2-D slices for the different object shapes (the full object for the 2-D snake), taken from *Set* 1/*Class-C* objects.

The analysis of pheromone maps for the definition of the segmentation performance will be described in detail later on.

5.1. Colony evolution

The colony population evolution is an interesting marker of the dynamical behaviour during the exploration process: Fig. 6 shows the evolution for the *Set* 1/*Class C* 1-*Arm-Bridge* and *toroid*. The evolution pattern is usually simple, with a triangular-like shape. However, when the anthill is placed along a thin long structure, as it is for the 1-*Arm-Bridge*, the peak structure appears later, since the population growth is prevented until the ants reach the thicker parts of the object.

The number of cycles before the colony extinction and the average population are summarized in Table 3 for the different object classes of *Set* 1. The colony life duration depends on the object complexity and size as well as on the anthill position (for example, the 1-*Arm-Bridge* is the last to be completed because the anthill is placed on the thin arm structure). However, an average trend can be observed if the same objects of *class A*, *B* and *C* are compared: the extinction is slightly quicker for objects with

Table 2
The properties of the simulated object sets.

Object set	*Class A*	*Class B/C*		*Class C*	
	Intensity	Average	Std. dev.	Baseline	Noise
Set 1	1300	700	200	100	50
Set 2	1600	700	300	100	50
Set 2	1000	700	100	100	25, 50, 75, 100
Set 3	–	700, 1050, 1400	200	100	50

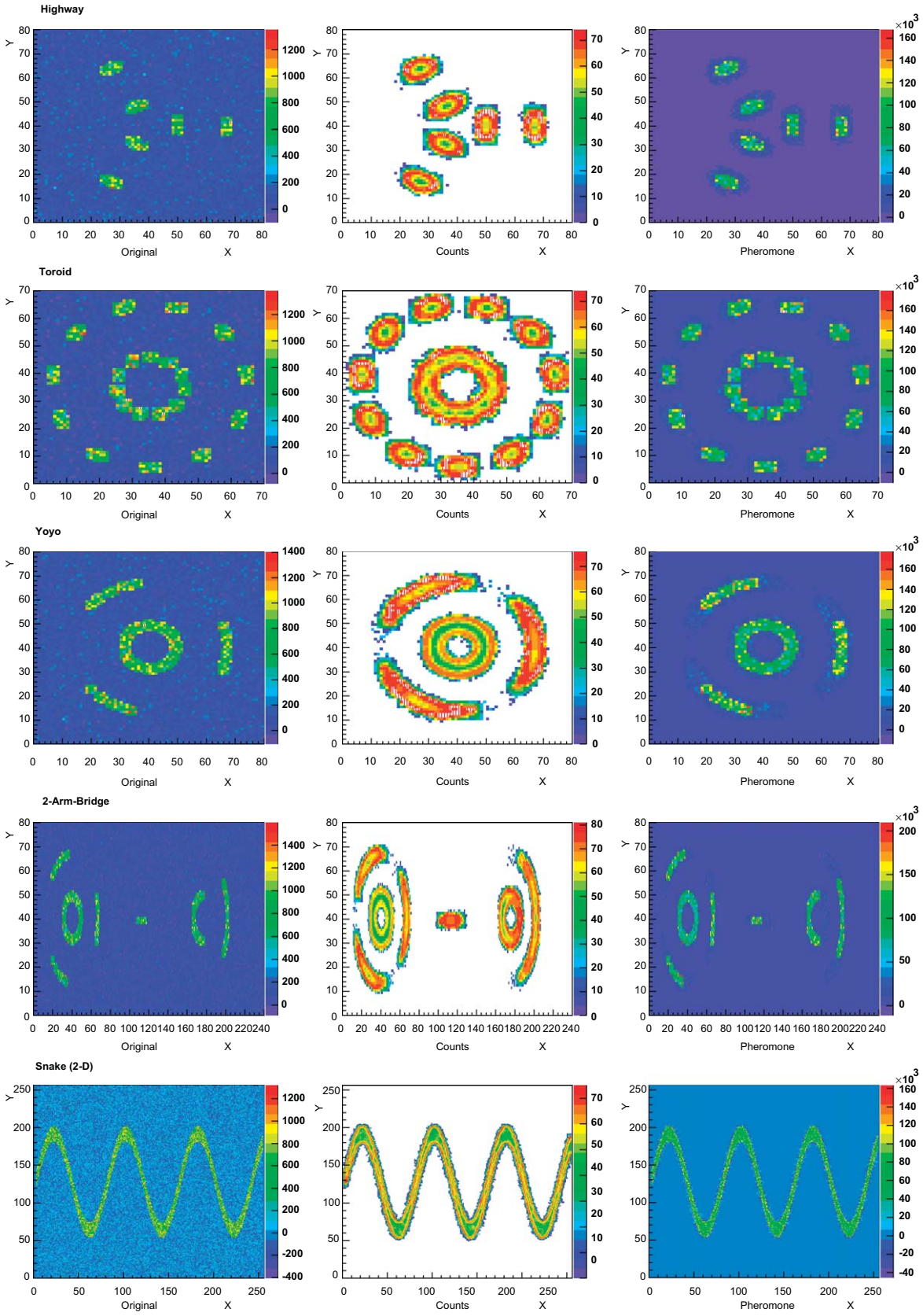

Fig. 5. Channeler Ant Model results on some *Set* 1/*Class-C* objects: (a) 2-D slice of the original image, (b) 2-D map of *voxels* visits, (c) 2-D section of the pheromone map. Row 1: the *highway*, row 2: *toroid*, row 3: *yoyo*, row 4: 2-*Arm-Bridge*, row 5: 2-*D snake*.

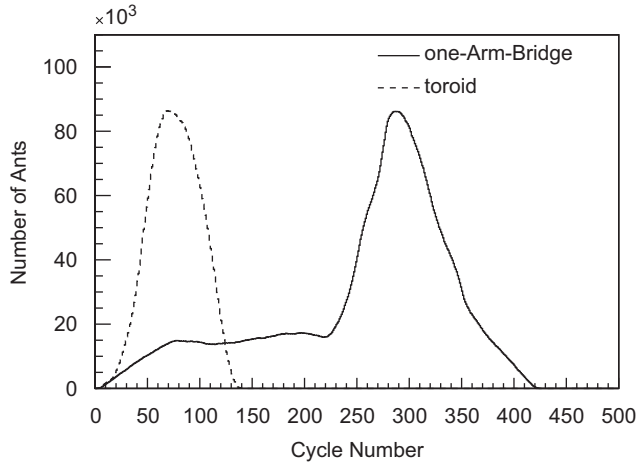

Fig. 6. The colony evolution: the population variation for the segmentation of the *Set* 1/*Class C* 1-*Arm-Bridge* and *toroid* as a function of the cycle number. The standard pattern is triangular-like, with the exception of the 1-*Arm-Bridge*, where the location of the anthill along the thin bridge limits the population increase until the thicker part of the object is reached.

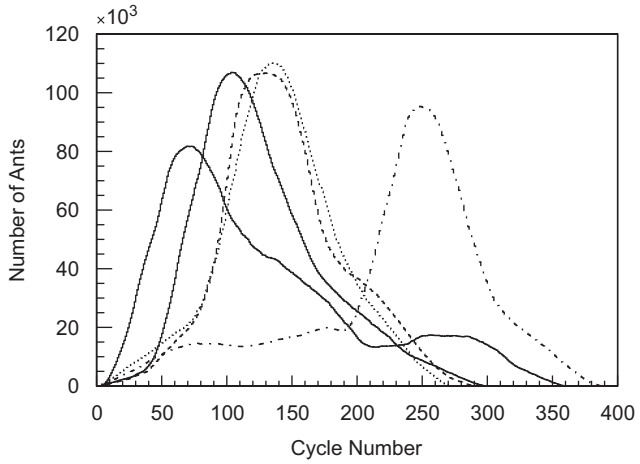

Fig. 7. Number of ants as a function of the cycle number for the segmentation of the 2-*Arm-Bridge* starting from different anthill positions. The ant colony evolution pattern is different, as expected, but the *sensitivity* and the *exploration level* are compatible and show that the CAM performance does not depend on the anthill location.

Table 3
The number of cycles the colony lives (N_{Cyc}) and the average number of ants per cycle ($\langle N_A \rangle$) for *class A*, *B* and *C* objects.

Object	*Class A*		*Class B*		*Class C*	
	N_{Cyc}	$\langle N_A \rangle$	N_{Cyc}	$\langle N_A \rangle$	N_{Cyc}	$\langle N_A \rangle$
Highway	141	8043	156	7867	162	8863
Scale	206	9365	224	9279	245	10061
Knot	143	20338	148	19394	147	22440
Toroid	139	34242	152	34347	142	40463
Yoyo	241	27050	254	27497	269	29039
1-*Arm-Bridge*	357	24338	367	25406	418	25683
2-*Arm-Bridge*	240	37051	251	37870	294	37090

uniform intensity (*class A*), while it takes a little longer (about 10% more cycles) when the intensity is not uniform (*class B*) and another 5–10% more when a Gaussian noise is added (*class C*). Also, the average number of ants in the colony increases by 10–15% when adding the noise.

These results are no different than what expected, given the model rules. The colony average population essentially depends on the pheromone levels, which in turn depend on the image *voxel* intensities: the change from uniform to variable (and lower, on average) intensity causes a slower population increase, and therefore requires a larger number of cycles to complete the segmentation.

The addition of a noisy background increases the average life of ants, since small pheromone quantities can be released outside the object and therefore the ant energy decrease outside the object is slower, turning into a larger average number of living ants.

The colony evolution is also a function of the anthill location: depending on the local object properties (i.e., the topology in the surroundings of the anthill), the number of ants in the colony shows different patterns, as seen in Fig. 7. The peak in the ant population is always reached when the thick arm structures are being explored. When the anthill is located on (or close to) the thin bridge connecting the two arms, the population reaches a plateau corresponding to the bridge exploration, and increases again when the ants reach the arms.

5.2. Object segmentation

As already remarked, the ant colony is deployed and evolves until its extinction, generating a pheromone map which represents the global knowledge of the environment. In order to evaluate the CAM performance with respect to the object segmentation, a definition of when *voxels* are to be considered as part of the object must be provided. We chose to use an *inclusion condition* that, applied to the pheromone map, generates a binary image: whenever a *voxel* contains more pheromone than a predefined threshold value (Ph_{th}), it is classified as *segmented*.

Therefore, the results are threshold dependent and, in principle, shape and set/class dependent.

The following analysis will show that the CAM provides uniform results as well as the possibility of defining a common threshold for the pheromone map analysis, which makes it suitable for the analysis of complex structures with *a priori* unknown intensities.

In order to quantify the model performance in the segmentation the following quantities were defined:

- *Sensitivity*: $S = N_R/N_O$, i.e., the ratio between the number of segmented *voxels*, evaluated with the pheromone map analysis, that actually are part of the object and the number of *voxels* in the original object;
- *Exploration level*: $E = N_V/N_O$, i.e., the ratio between the number of segmented *voxels* and the number of *voxels* in the original object;
- *Contamination*: $C = N_C/N_O$, i.e., the ratio between the number of segmented *voxels* that do not belong to the original object and the number of *voxels* in the original object, after the pheromone map analysis.

According to the definitions:

$$C = (N_V - N_R)/N_O = E - S \tag{12}$$

S, E and C are function of the threshold value: however, if the model in general enough, they shall not be object shape dependent.

Fig. 8 shows the *exploration level* (E) and *sensitivity* (S) for the *Set* 1/*Class A*, *B* and *C highway* as a function of the selected pheromone threshold. For *class A* and *B* objects, the *exploration level* and the *sensitivity* are coincident, since the pheromone

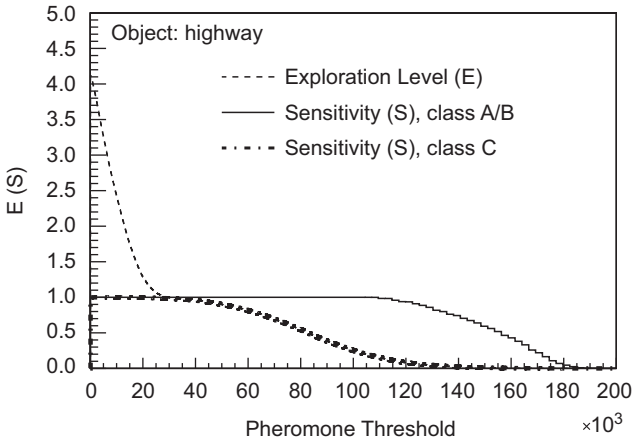

Fig. 8. *Set* 1/*Class A*, *B* and *C highway*: *exploration level* (*E*, only for *Class C*) and *sensitivity* (*S*) as a function of the selected pheromone threshold. The *exploration level* for the A, B classes is equal to the *sensitivity*, since there is no background; for the C class, it merges with the *sensitivity* as the pheromone threshold increases.

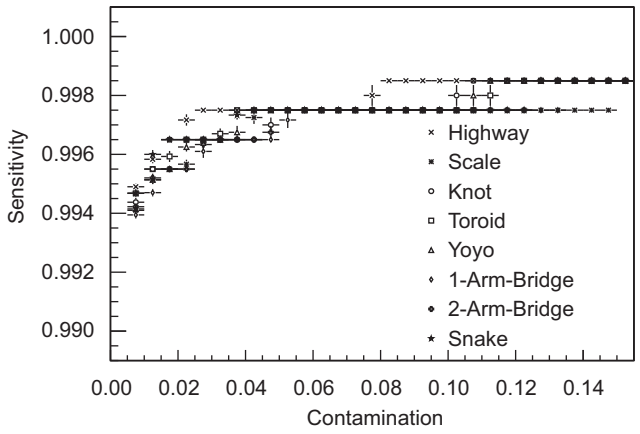

Fig. 9. *Set* 1/*Class C* objects: the correlation between the *sensitivity* and the *contamination* (*S*) shows that the CAM performance is independent of the shape within a *sensitivity* range of 0.001.

Table 4
Pheromone threshold Ph_{th} and contamination *C* corresponding to $S = 0.999$ (left side); pheromone threshold Ph_{th} and sensitivity (*S*) corresponding to $C = 0.01$ (central part); pheromone threshold Ph_{th} and contamination *C* corresponding to $S = 0.99$ (right side).

Object	$S = 0.999$		$C = 0.01$		$S = 0.99$	
	Ph_{Th}	*C*	Ph_{Th}	*S*	Ph_{Th}	*C*
Highway	16900	0.52	30700	0.996	37200	0.0004
Scale	16700	0.64	31300	0.995	37400	0.0007
Knot	18200	0.41	31500	0.995	36700	0.0011
Toroid	17500	0.42	30100	0.995	36000	0.0007
Yoyo	16300	0.48	30700	0.995	36500	0.0007
1-Arm-Bridge	17100	0.48	31300	0.994	37300	0.0007
2-Arm-Bridge	17900	0.41	30900	0.995	37000	0.0009
Snake 2D	13900	0.34	28300	0.995	35300	0.0013

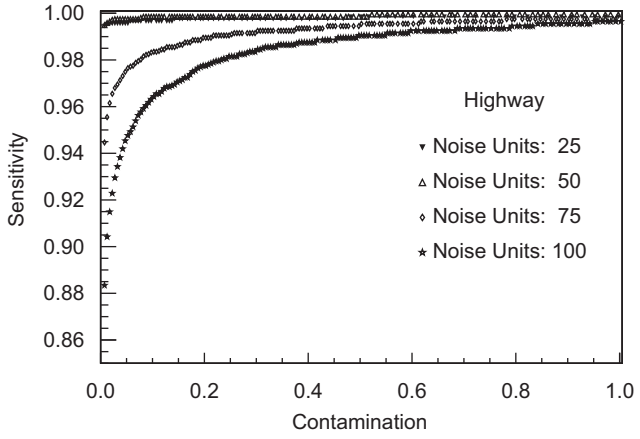

Fig. 10. Correlation between the *sensitivity* and the *contamination* for the *Set* 1/*Class C* highway (average intensity 700, standard deviation 200) as a function of the selected pheromone threshold for different noise values.

release that takes place when the *voxel* intensity is zero is so small that falls below the smallest threshold value. It is interesting to observe that adding the noise does not affect the segmentation capability (the *class B*, *C* sensitivity curves are almost the same) while, as expected, it introduces a contamination, caused by the pheromone release in *voxels* that do not belong to the object.

Given the trend shown in Fig. 8 and the correlation between Ph_{th}, *S* and *C*, three points, defined by the conditions $S = 0.999$, $C = 0.01$ and $S = 0.99$, were selected as representative of the CAM performance. Table 4 shows, for the different artificial objects of *Set* 1/*Class C*, the values of Ph_{th} and *C* corresponding at $S = 0.99$ on the left side, Ph_{th} and *S* at $C = 0.01$ in the central part and Ph_{th} and *C* at $S = 0.99$ on the right side. The threshold interval between the values at $C = 0.01$ and $S = 0.99$ defines the range corresponding to a satisfactory performance.

Since the sensitivity and contamination are evaluated at each pheromone threshold value, it is also possible to study their correlation with a more general approach. The curves obtained by varying the pheromone threshold and plotting the sensitivity as a function of the contamination for the different shapes on the *Set* 1/*Class C* objects (Fig. 9) show that the CAM performance is independent of the shape within a sensitivity range of 0.001 and therefore the model is general enough to segment different objects with similar sensitivity and contamination levels.

It is then essential to study the model behaviour as a function of the intensity range and the noise level. The correlation between the *sensitivity* and the *contamination* for the *Set* 2/*Class C* highway at different noise levels, shown in Fig. 10, shows—as expected—that the performance improves as the noise level decreases.

The noise level is the most important parameter in discriminating the CAM performance with respect to other algorithms. Since the CAM output (i.e., the pheromone map) is analysed with a simple thresholding, a comparison to a simple thresholding on image intensity provides a measurement of the improvement introduced by the CAM. Fig. 11 shows the results for the two approaches on a highway with different noise levels: the larger the noise, the better is the CAM result with respect to the simple thresholding.

That is somehow expected, since in the CAM the channelling features allow the rejection of high intensity *voxels* that are far from the structure being segmented.

In order to compare the CAM results to a more sophisticated and performing algorithm, a region growing-based (RG) approach [26] was selected, because of its similarities with the CAM in exploring connected structures in a 3-D environment.

Basically, the RG algorithm segments structures starting from a seed point (equivalent to the CAM anthill) and providing *inclusion rules* that allow to deterministically decide whether a *voxel* should be considered as part of the analysed structure or not. Fig. 12 shows

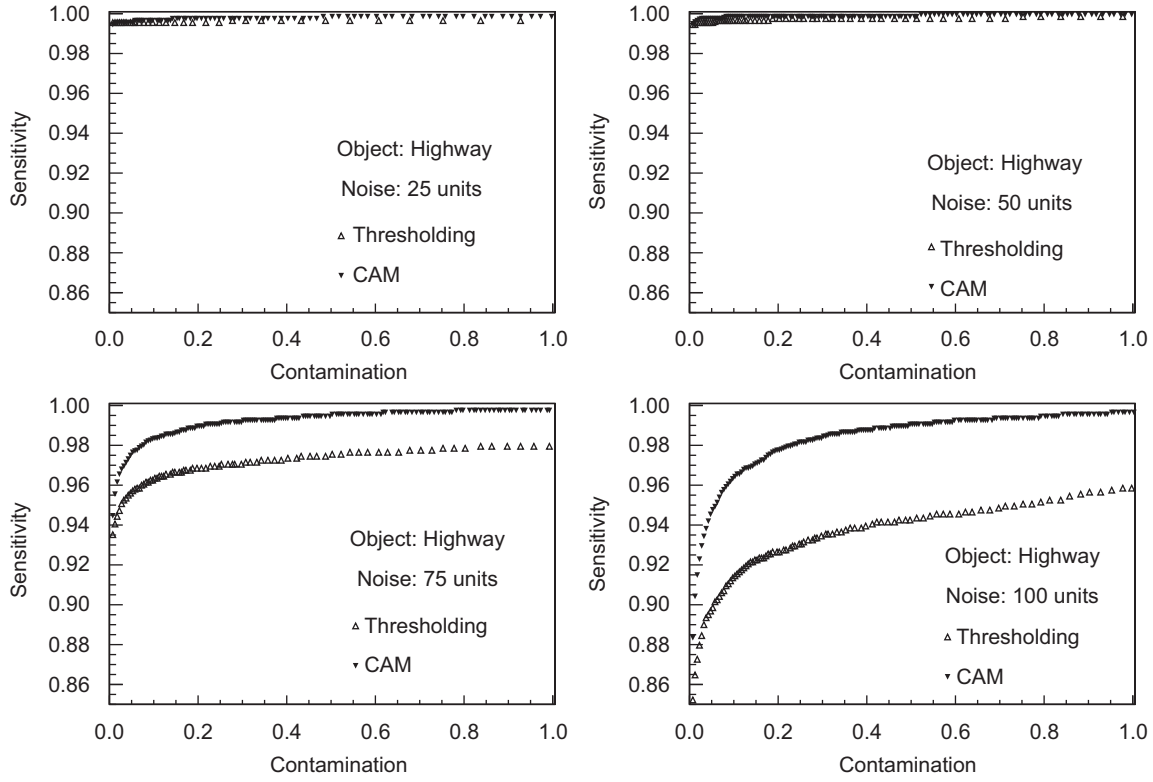

Fig. 11. Correlation between the *sensitivity* and the *contamination* for the *Set* 1/*Class C* highway (average intensity 700, standard deviation 200) at different noise levels, for the CAM with simple threshold analysis of the pheromone map and a simple thresholding algorithm on the image intensity.

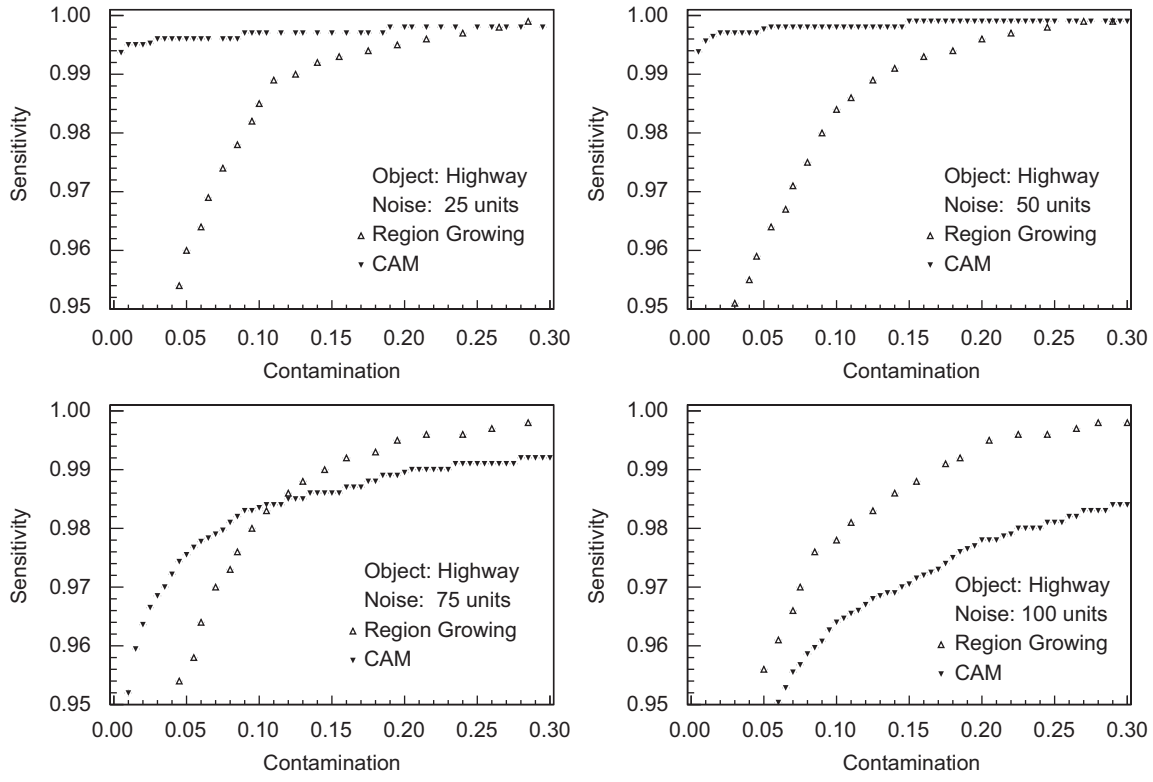

Fig. 12. Correlation between the *sensitivity* and the *contamination* for the *Set* 1/*Class C* highway (average intensity 700, standard deviation 200) at different noise levels, for the CAM with simple threshold analysis of the pheromone map and a double thresholding (on intensity) Region Growing algorithm.

the comparison for the different noise levels: it is interesting to observe that, while the performance of the CAM decreases (i.e., the contamination increases) with the noise, the RG result is very stable. Such a behaviour is strictly related to the fact that the RG decision is made once and for all while exploring the original image, while the CAM progressively stores information in the pheromone map which is analysed after the colony extinction. The RG does not suffer such from a noise increase, since its exploration in a given direction abruptly stops when just one voxel is below threshold. On the other hand, the CAM behaviour is regulated by the ant energy, which allows exploration ranges outside the object that increase with the noise level. Overall, the CAM performance is better when the noise is lower (since the RG anyhow misses a fraction of the object *voxels*) while the RG is better at higher noise values.

Such differences can be overcome by introducing a slightly more sophisticated analysis that takes into account for the CAM (RG) the *voxel* pheromone amount (intensity) and its average in a $3 \times 3 \times 3$ box around it. The results (Fig. 13) show the performance of the CAM when only the average pheromone quantity is taken into account and of the RG when both the *voxel* intensity and its average with first order neighbours are used for thresholding. The improvement is remarkable, to the extent of being extremely close to a 100% sensitivity for all the noise values in a much lower range of contamination values (note that also the *x*-axis scale differ in Figs. 11–13).

Both the RG and the CAM, therefore, prove to be very performant. However, there is an interesting CAM feature that could make it preferable to RG. While the RG analysis parameters (i.e., the lower and upper thresholds that are used by the *voxel* inclusion rules) operate on the image intensity and therefore must be tuned whenever the original intensity range changes, the CAM analysis parameter (i.e., the pheromone threshold) does not depend on the intensity range, as seen in Fig. 14, that shows the effect of an increasing signal values at constant noise on the *exploration level* and *sensitivity* for the *Set* 3/*Class C* 2-*Arm-Bridge*. The distribution shows that there is no effect on E and S at low pheromone thresholds, while the plateau with negligible contamination and full segmentation progressively extends: in other words, as long as the pheromone threshold is selected for the worst signal to noise ratio, the segmentation capability is not affected by increasing the signal range. The *CAM* behaviour as a function of the noise at a given average intensity (or, in other words, as a function of the average intensity to noise ratio) shows that, unless the noise levels are very high, it is possible to define a

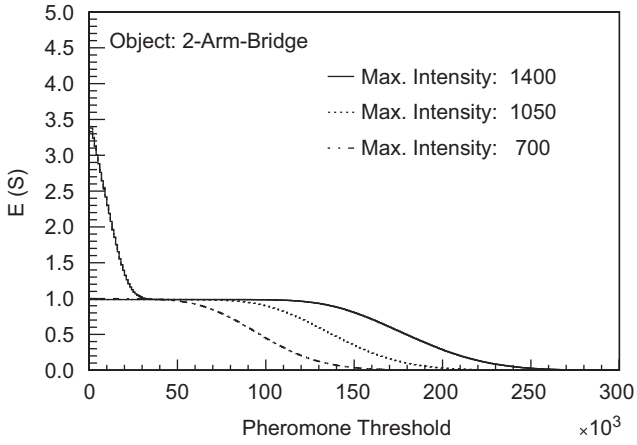

Fig. 14. *Exploration level* (E) and *sensitivity* (S) as a function of the selected pheromone threshold for the *Set* 3/*Class C* 2-*Arm-Bridge* with increasing average intensity, at constant standard deviation, noise and baseline (i.e., increasing signal to noise ratio).

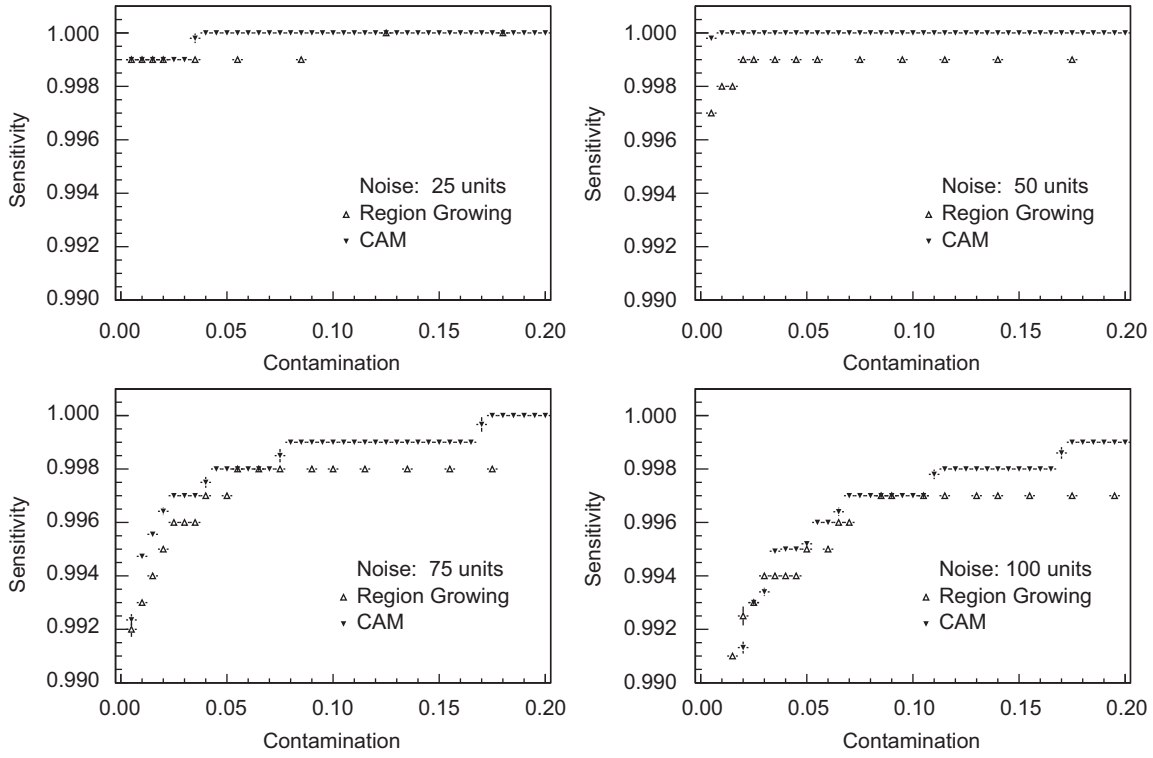

Fig. 13. Correlation between the *sensitivity* and the *contamination* for the *Set* 1/*Class C* highway (average intensity 700, standard deviation 200) at different noise levels, for the CAM with simple threshold analysis of the averaged pheromone map and a double thresholding (on intensity and averaged intensity) Region Growing algorithm. By *averaged* it is meant that both the pheromone quantities and the image intensities are replaced by the average of a $3 \times 3 \times 3$ cell (i.e., the *voxel* and its first order neighbours).

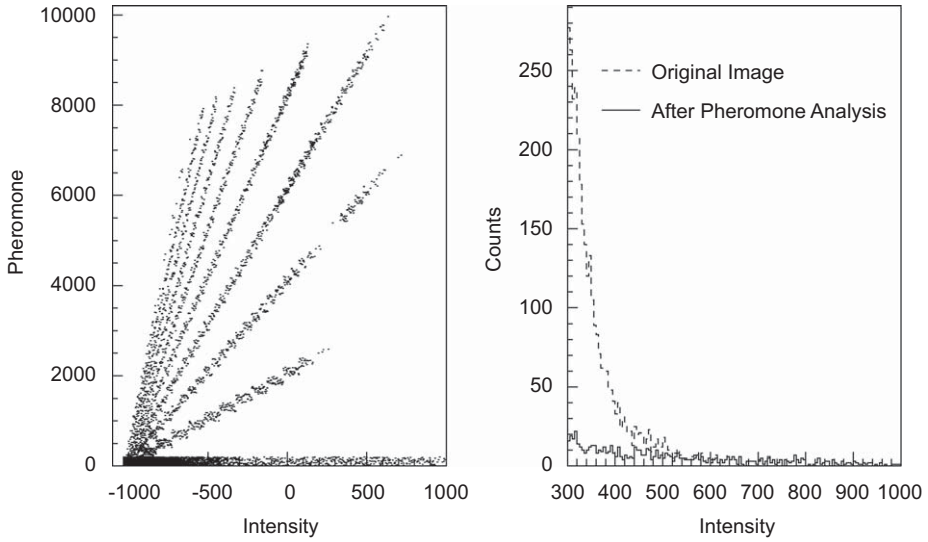

Fig. 15. *Pheromone level* as a function of the *intensity* for a lung computed tomography of $512 \times 512 \times 313$ size (left). Intensity distribution of the set of voxels with *Intensity* > 300 units and pheromone level < 1000 (right).

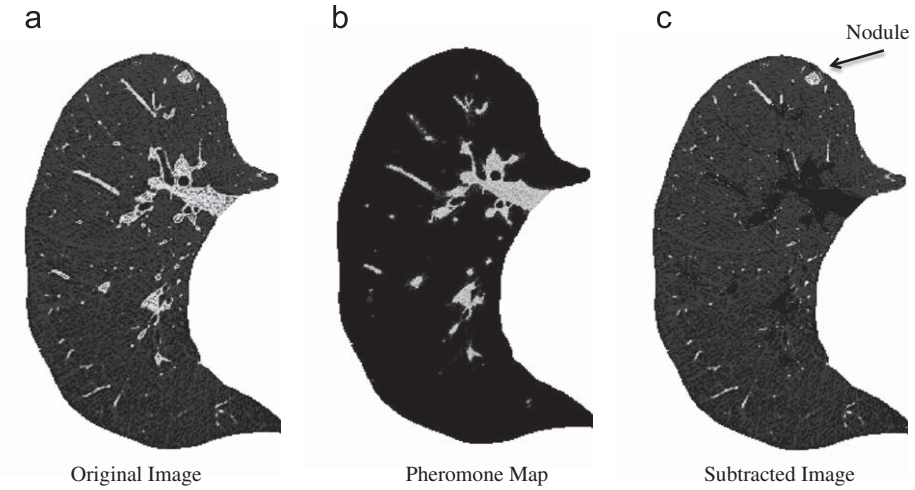

Fig. 16. An example of the CAM results on a 2-D slice of a lung CT: original image (a), pheromone map (b) and *subtracted* image (c).

range of pheromone threshold values for which the segmentation is fully satisfactory.

5.3. Lung CT analysis

Although it is not easy to define a quantitative performance when the CAM is deployed on lung computed tomographies, it is nevertheless interesting to assess its behaviour on a qualitative level. When analysing a CT, the anthill is set at the root of the bronchial and vascular trees, and the colony environment is defined by the voxels accepted by the lung volume segmentation module. The right and left lungs are analysed separately, since they are by definition topologically disconnected. The pheromone release rule is defined in such a way that the release is proportional to the difference between the voxel intensity and the minimum intensity in the lung volume. Fig. 15 (left) shows the correlation between the pheromone level and the original intensity of each voxel. The straight structures correspond to different numbers of visits to a voxel during the colony evolution. Most of the voxels lay at the bottom, not having been visited by the ants and therefore containing no pheromone. For some of them, however, the intensity can be very large: these voxels are the best candidates as belonging to a nodule, which is most of the time a high intensity object topologically disconnected from the bronchial and vascular tree. Fig. 15 (right) shows the comparison between the intensity distribution of the voxels with $I > 300$ units in the original image (dashed line) and after the CAM deployment and pheromone analysis (full line): as compared to the original image, the number of accepted voxels has been reduced by a large factor, particularly for medium intensities ($300 < I < 500$).

The result of the CAM deployment on a slice of a CT containing a nodule to be detected is shown in Fig. 16: after resetting the voxels with a pheromone content above threshold (b), the original image (a) turns into the so-called *subtracted* image (c), where the nodule to be detected is much easier to spot without false findings.

The *subtracted* image becomes the input object to the filtering stage that looks for nodule candidates and classifies them. A detailed discussion of its features and results is beyond the scope of this work: it is addressed in [11,12], which describe the goal and the results of the ANODE09 challenge [13].

6. Conclusions and prospects

Artificial ant-colonies have been used in image processing for over a decade, but most of the existing algorithms and models deal with 2-D image segmentation, thresholding or processing problems. Some approaches treating and using the full capabilities of self-organization, trail forging and nest building in an ant colony in 3 dimensions do exist. However, to our knowledge, none of these try to model these capabilities in 3-D image processing.

Since real-ants in nature perform unknown, uncharted object recognition every day and they carry on 3-D object construction in the activity of nest building, artificial ant colonies should be able to do the same.

The Channeler Ants Model describes ants in terms or rules that define their moving capabilities, the pheromone release, the life cycle (birth, reproduction, death) and the deviating behaviours. It proves to be suitable for a full segmentation of objects of different shape, intensity range in a noisy background.

The property of channelling appears as an emergent behaviour of the entire colony, which propagates in the 3-D image, its population being controlled by the energy depletion, until the full structure is explored and the colony extinguishes.

The Channeler Ant Model performance was successfully validated on artificial images, without any parameter tuning when the image or the environment properties changed.

Moreover, a preliminary analysis of lung computed tomographies shows that the CAM is suitable for use as part of a Computer Assisted Detection tool for the automated detection of nodules in the lung.

Acknowledgement

The authors wish to thank the *Associazione per lo Sviluppo Scientifico e Tecnologico del Piemonte* for contributing to the work with a grant.

References

[1] E. Bonabeau, M. Dorigo, G. Theraulz, Swarm Intelligence, from Natural to Artificial Systems, Oxford University Press, Oxford, 1999.
[2] M. Dorigo, V. Maniezzo, A. Colorni, The ant system: optimization by a colony of cooperating agents, IEEE Transactions on Systems, Man and Cybernetics B 26 (1996) 29–41.
[3] 〈http://www.swarm-bots.org.〉.
[4] D. Chialvo, M. Millonas, How swarms build cognitive maps, The Biology and Technology of Intelligent Autonomous Agents 144 (1995) 439–450.
[5] X. Zhuang, N.E. Mastorakis, Image processing with the artificial swarm intelligence, WSEAS Transactions on Computers 4 (2005) 333–341.
[6] L. Bocchi, L. Ballerini, S. Hassler, A new evolutionary algorithm for image segmentation, in: EuroGP 2005—EvoWorkshops 2005, Lecture Notes in Computer Science, Springer, Berlin, 2005, pp. 39–43.
[7] A. Malisia, H. Tizhoosh, Image thresholding using ant colony optimization, in: The 3rd Canadian Conference on Computer and Robot Vision, vol. 3, 2006, p. 26.
[8] J. Liu, Y. Tang, Adaptive image segmentation with distributed behaviour-based agents, IEEE Transaction on Pattern Analysis and Machine Intelligence 21 (1999) 544–551.
[9] E.O. Wilson, B. Holldobler, The Ants, Harvard University Press, Cambridge, MA, 1990.
[10] R. Bellotti, et al., Distributed medical images analysis on a grid infrastructure, Future Generation Computer Systems 23 (2007) 475–484.
[11] B. Van Ginneken, Automatic NOduleDEtection, in: SPIE2009 Conference, Lake Buena Vista (Orlando Area), FL, USA, 7–12 February 2009.
[12] B. Van Ginneken, et al., Comparing and combining algorithms for computer-aided detection of pulmonary nodules in computed tomography scans: the ANODE09 study, Medical Image Analysis, submitted for publication.
[13] 〈http://anode09.isi.uu.nl/〉.
[14] J.-L. Deneubourg, S. Aron, S. Goss, J.-M. Pasteels, The self-organizing exploratory pattern of the argentine ant, Journal of Insect Behavior 3 (1990) 159–168.
[15] J.-L. Deneubourg, N.R. Franks, S. Goss, J.-M. Pasteels, The blind leading the blind: modelling chemically mediated army ant raid patterns, Journal of Insect Behavior 2 (1989) 719–725.
[16] E. Bonabeau, G. Theraulz, J.-L. Deneubourg, Quantitative study of the fixed threshold model for the regulation of division of labor in insect societies, Proceedings of the Royal Society London B 323 (1996) 1565–1569.
[17] J.-L. Deneubourg, S. Goss, A. Sendova-Franks, C. Detrain, L. Chretien, The dynamics of collective sorting: robot-like ant and ant-like robot, Proceedings First Conference on Simulation of Adaptive Behavior, vol. 1, MIT Press, Cambridge, MA, 1991, pp. 356–365.
[18] P.-P. Grasse, Termitologia, Tome II. Fondation des Societes. Construction, Masson, Paris, 1959.
[19] V. Ramos, F. Almeida, Artificial ant colonies in digital image habitats—a mass behaviour effect study on pattern recognition, in: Proceedings of ANTS 2000—2nd International Workshop on Ant Algorithms (From Ant Colonies to Artificial Ants), Belgium, 2000, pp. 39–43.
[20] V. Ramos, C. Fernandes, A.C. Rosa, Self-regulated artificial ant colonies on digital image habitats, in: Proceedings of the ICANN'05: 15th International Conference, Lecture Notes in Computer Science, vol. 3696, Springer, Berlin, 2005, pp. 311–316.
[21] V. Ramos, C. Fernandes, A.C. Rosa, Varying the population size of artificial forging swarms on time varying landscapes, in: Proceedings of the ICANN'05: 15th International Conference, Lecture Notes in Computer Science, vol. 3696, Springer, Berlin, 2005, pp. 311–316.
[22] F. Meyer, Skeletons and perceptual graphs, Signal Processing 16 (1989) 335–363.
[23] P. Khajehpour, C. Lucas, B. Araabi, Hierarchical image segmentation using ant colony and chemical computing approach, in: Advances in Natural Computation, vol. 3611, Springer, Berlin, 2005, p. 1250.
[24] C. George, J. Wolfer, A swarm intelligence approach to counting stacked symmetric objects, in: Artificial Intelligence and Applications, Acta Press, Austria, 2006.
[25] E.F. Moore, Gedanken experiments on sequential machines, Automata Studies, 1956.
[26] R. Bellotti, et al., A CAD system for nodule detection in low-dose lung CTs based on region growing and a new active contour model, Medical Physics 34 (12) (2007) 4901–4910.

About the Author—PIERGIORGIO CERELLO graduated in Physics in 1989 at the University of Torino. After 2 years spent at CERN, he started a Ph.D. in Physics, completed in 1995 at the University of Torino. He is a member of the CERN/ALICE Project, with contributions in the area of interfaces to Grid Services and software for the silicon drift detectors. Since 2003 he is Project Coordinator of MAGIC-5, focused on the developments of software for the automated detection of anomalies in medical images, to be used in a distributed environment.

About the Author—SORIN CRISTIAN CHERAN has graduated in 2003 in Computer Science Faculty from Politehnica University of Bucharest. Holds a Ph.D. in Computer Science obtained in 2007 from the Universita degli Studi di Torino. Presently he is working for Hewlett Packard EMEA as a High Performance Computing Engineer and Solution Architect.

About the Author—STEFANO BAGNASCO graduated in Physics in 1996 from University of Torino, Italy and, after one year at Fermilab, obtained his Ph.D. in 2001 from University of Genova, Italy, working on the BaBar experiment. He is currently working in the context of the ALICE experiment at CERN and of the European Grid initiative EGEE. He has also worked on the development of an interface to Grid Service of a mammogram analysis station.

About the Author—ROBERTO BELLOTTI graduated in Physics at the University of Bari in 1988. He is presently Associate Professor of Experimental Physics at the University of Bari, Italy. His research takes place in the areas of Medical Physics, where he took part in the development of CAD systems for the breast and lung cancer detection, and Experimental Physics.

About the Author—LOURDES BOLANOS is a Researcher at the CEADEN, Habana, Cuba. She spent one year as University of Torino fellow at INFN, Torino and worked on the manuscript review as well as on the use of the Channeler Ant Model for the analysis of lung computed tomographies.

About the Author—EZIO CATANZARITI is Associate Professor of Computer Science at the Faculty of Sciences of Università di Napoli Federico II. His research interests span the fields of computer vision, computational models of brain, remote sensing and pattern recognition with special focusing on medical image analysis, automated diagnosis and recognition and control of object-directed actions.

About the Author—GIORGIO DE NUNZIO received the Master's degree in Physics from the University of Salento (Lecce, Italy) (1991), and a Ph.D. from the University of Montpellier II (1995). Since 2001 he is with the University of Salento, where he is Researcher in Applied Physics. His research interests focus on physics, informatics, and image processing, applied to medicine and cultural heritage.

About the Author—MARIA EVELINA FANTACCI is a Researcher of Medical Physics at the University of Pisa. Main interests in the development of algorithms for the Computer Assisted Detection of signatures in medical images.

About the Author—ELISA FIORINA graduated in Physics at the University of Torino in 2007 with a thesis on the Channeler Ant Model performance on artificial objects.

About the Author—GIANFRANCO GARGANO graduated in Physics in 2001 and got a Ph.D. in Physics in 2006 at the University of Bari. Since 2003 his research activity focuses on the development of Computer Aided Detection Systems lung nodules in CT scans.

About the Author—GIANLUCA GEMME got his Master degree in Physics in 1989, at the University of Genoa. In 1993 he got a permanent position as Technical Scientist at INFN and since 2003 he has been Senior Researcher at INFN. Since 2005 he joined the research program Magic-5 (Medical Application on a Grid Infrastructure Connection) of INFN.

About the Author—ERNESTO LÓPEZ TORRES graduated in Nuclear Physics at the Instituto Superior de Ciencias y Tecnología Nucleares, Cuba, in 1991. He is presently working on the Monte Carlo Simulation and particle transport in the ALICE experiment at CERN and on the use of Ant Colonies for the object segmentation on artificial objects and medical images.

About the Author—GIOVANNI LUCA MASALA graduated in Electronic Engineering in 2002; he completed a Ph.D. in Physics in 2006. His research activities are in the field of Physics Applied to Medicine and Pattern Recognition.

About the Author—CRISTIANA PERONI is a Professor of Medical Physics at the University of Torino. Research activity in medical physics, with main interests in the development of devices for the dosimetry and monitoring of therapeutical beams of photons, electrons and hadrons in collaboration with research centers and with industry.

About the Author—MATTEO SANTORO obtained a Ph.D. in Computer Science and a Degree in Physics from the University of Naples (Italy). Currently, he is a post-doc at DISI, University of Genova (Italy), where his research work aims at building knowledge discovery and decision support systems based on the multi-modal integration of biomedical information. His main interests are: statistical inference, machine learning and inverse problems for biomedical data analysis.